# Modeling Heat Conduction in Nanoporous Silicon with Geometry Distributions

Makoto Kashiwagi, Yuta Sudo, Takuma Shiga, and Junichiro Shiomi

Phys. Rev. Applied **10**, 044018 — Published 5 October 2018

DOI: 10.1103/PhysRevApplied.10.044018

# Modelling heat conduction in nanoporous silicon with geometry distributions

Makoto Kashiwagi[1], Yuta Sudo[1], Takuma Shiga[1], and Junichiro Shiomi[1*]

[1]*Department of Mechanical Engineering, The University of Tokyo, 7-3-1 Hongo, Bunkyo, Tokyo, 113-8656, Japan*

* Email address: shiomi@photon.t.u-tokyo.ac.jp

**Abstract**

Formation of nanoporous structures is an effective approach to manipulate heat conduction and has been experimentally demonstrated to largely reduce thermal conductivity. Thermal conductivity reduction of nanoporous materials depends on structural parameters such as size, shape and position of the pores, and their distributions, which are hard to explore in experiments. In this work, by systematically performing ray-tracing Monte Carlo simulations of nanoporous silicon crystal, we have evaluated impacts of the structural parameters on the thermal conductivity reduction. As a result, we found that the thermal conductivity reduction with spherical pores is insensitive to the spatial configuration and size distribution of the pores, even in the regime of quasi-ballistic phonon transport. Although the sensitivity does increase as phonon scattering by the pores becomes directional as for rectangular pores and porosity increases, the overall results deliver aspects that are useful in practice: the thermal conductivity of nanoporous structures can be well described by a phonon scattering model with a single length scale.

## I. Introduction

Influence of pores on lattice heat conduction through a solid is important in developing thermal-functional semiconductors and insulators. Particularly nanoscale pores are omnipresent in materials produced by processes that involve nucleation, deformation, and phase transition. Presence of pores reduces thermal conductivity, which can be good or bad depending on the application and situation. A case that benefits from the reduction for instance is thermoelectrics that enables direct conversion between heat and electricity. Thermoelectric figure-of-merit of a material can be expressed as $zT=(S^2\sigma/\kappa)T$, where $S$, $\sigma$, and $\kappa$ are Seebeck coefficient, electrical conductivity, and thermal conductivity at a given temperature $T$ [1]. In the course of aiming to enhance $zT$ by reducing thermal conductivity, there have been a number of reports that formed nanostructures in materials by sintering [2], deposition [3], or precipitation [4,5]. The process typically results in nanoscale pores whether intentionally or unintentionally, which also contributes to suppressing thermal conductivity.

The way nanostructures influence heat conduction depends on their geometries. For instance, in polycrystalline materials with nanoscale grains (nanocrystalline materials), the grain boundaries potentially suppress heat conduction by scattering phonons with mean free path (MFP) larger than the grain size. Here, the actual problem is more complex because heat is carried by a wide range of phonons with different modes (wavevectors and branches) and thus MFPs, which makes the suppression mode-dependent and multiscale. These dependences of the scattering on phonon modes and structure size also apply to pores, however, the extent of reflection is clearly different; pores perfectly prohibit phonon propagation, whereas grain boundaries allow transmittance particularly of phonons with long MFP (low frequency). Note that

transmittance of long-wavelength phonon is almost one even at incoherently-bonded grain boundaries [6]. Therefore, pores have potential to cause larger thermal conductivity reduction, which may be beneficial for applications such as thermoelectrics if that can be done without appreciably sacrificing electrical conductivity by utilizing the MFP difference between phonons and electrons.

Thermal conductivity reduction by nanopores has been experimentally measured particularly for thermoelectric materials. Boor *et al*., fabricated nanoporous silicon (Si) crystal by means of an electrochemical etching, and reduced thermal conductivity to 5% of bulk Si thermal conductivity [7]. Takashiri, *et al.*, made nanoporous-nanocrystalline $Bi_2Te_3$ by sintering and 90% reduction of thermal conductivity was achieved even though the intrinsic thermal conductivity of bulk $Bi_2Te_3$ is as small as 1.5 W/m-K at room temperature [8,9]. Song, *et al*., applied the liquid phase deposition method to bismuth and fabricated porous Bi structure with extremely low thermal conductivity [4]. However, electrical conductivities in these samples were also noticeably reduced, and consequently $zT$ enhancement was limited. In contrast, by means of lithography technique and self-assembly structures as a template, holey thin films have been fabricated and shown to possess large $zT$ (0.4 at 300 K for Si [10] and 1.8 at 300 K for $Bi_2Te_3$ [3]).

To predict and understand the effect of nanopores on thermal conductivity for further materials development, there is a need for a theoretical model that represents the effect of nanopores with geometrical distributions. Numerous theoretical models based on effective medium theories (EMT) such as Eucken model [11] and Bruggeman model [12,13] have been used to predict effective thermal conductivity ($\kappa_{\text{eff}}$) of porous materials [14]. These models are expressed as

$$\frac{\kappa_{\text{eff}}}{\kappa_{\text{bulk}}} = \frac{2-2\varphi}{2+\varphi}, \tag{1}$$

$$\frac{\kappa_{\text{eff}}}{\kappa_{\text{bulk}}} = \frac{(2-3\varphi)+|2-3\varphi|}{4}. \tag{2}$$

Here, $\kappa_{\text{bulk}}$ is the thermal conductivity of bulk Si, and $\varphi$ denotes a volume fraction of void. In these models, reduction in thermal conductivity is merely a function of volume fraction and independent of the geometry of each pores. Although, these models show good agreement with the effective thermal conductivity of micron-sized porous materials, they cannot predict the effective thermal conductivity of nanoporous materials with nanopores smaller than the intrinsic MFPs of phonon-phonon scattering since thermal conductivity of quasi-ballistic phonons strongly depends on the distance between the interfaces, and thus the geometry.

A model that takes phonon scattering into account from microscopic viewpoint is proposed by Kim and Majumdar [15]; which has been used to describe phonon scattering by nanoparticles [15-19].

$$\Lambda_{\text{pore}}^{-1} = \frac{n}{\sigma_s^{-1} + \sigma_l^{-1}}. \tag{3}$$

Here, $\sigma_s$ and $\sigma_l$ represent scattering cross-sections in the limits of short-wavelength and long-wavelength, respectively, and $n$ is the number density of pores. Although the validity of the phonon-nanoparticle scattering model has been verified by Monte Carlo and molecular dynamics simulations for nanoporous systems with several geometrical parameters such as pore size, shape, alignment, and volume fraction [20,21], in typical materials, those geometrical parameters are not uniform in space, and thus the validity and robustness of the model is still an open question. Therefore, in this work, we have evaluated the impacts of the geometrical parameters and their distributions in reducing thermal conductivity by systematically performing the ray-tracing

Monte Carlo (RTMC) simulations [22-24] for two kinds of Si-based nanoporous structures (spherical and rectangular pores) illustrated at Fig. 1.

## II. Method

On the basis of the kinetic gas theory, effective thermal conductivity ($\kappa_{\text{eff}}$) of nanoporous structure is given by [25]

$$\kappa_{\text{eff}} = \frac{1}{3}\sum_{s}\int_{\omega} C_s(\omega) v_s(\omega) \Lambda_{\text{eff},s}(\omega) d\omega, \tag{4}$$

where $C_s(\omega)$, $v_s(\omega)$, and $\Lambda_{\text{eff},s}(\omega)$ are respectively specific heat including density of states, group velocity, and effective MFP of phonon with angular frequency $\omega$ and branch $s$. $\Lambda_{\text{eff},s}(\omega)$ includes not only intrinsic phonon-phonon scattering but also phonon-pore scattering. Defining MFPs of phonon-phonon and phonon-pore scatterings with $\Lambda_{\text{bulk}}$ and $\Lambda_{\text{pore}}$ and adopting the Matthiessen's rule [25], $\Lambda_{\text{eff}}$ is expressed as

$$\Lambda_{\text{eff}}^{-1} = \Lambda_{\text{bulk}}^{-1} + \Lambda_{\text{pore}}^{-1}. \tag{5}$$

In this work, $\Lambda_{\text{pore}}$ for spherical and rectangular pores were calculated by using RTMC simulation. As illustrated in Fig. 1, this method calculates a transmittance ($\tau(\theta,\varphi)$) of incident phonon with azimuthal angle $\varphi$ and polar angle $\theta$ by counting the number of phonons reaching the *x*-*y* plane at $z=L$. Here, phonons enter the material at $z=0$ on *x*-*y* plane, where an incident azimuthal and polar angles are randomly chosen. In the case that pores are uniformly distributed on the *x*-*y* plane, the transmittance only depends on the polar angle ($\tau=\tau(\theta)$). In the calculation, phonon-pore scattering is treated as diffusive, which means that phonons are scattered diffusively in all directions uniformly (i.e. a random direction) without reference to the direction of the incident radiation [26].

As for the outer boundaries of the simulation cell, specular reflection condition is applied to the walls normal to the *x*- and *y*-axes, which is equivalent to having periodic boundary condition in the sense that the boundaries do not inhibit phonon/thermal transport. The side length of cross-section and length along the *z*-direction are respectively set to ten times the pore diameter and 20 μm, which is so long that transmittance is well converged. Under the detailed balance [27], combination of the Landauer formula and Boltzmann-Peierls equation leads to the expression for $\Lambda_{\mathrm{pore}}$ by the $\tau(\theta)$ [24]

$$\Lambda_{\mathrm{pore}} = \frac{3L}{2}\int_0^{\pi/2} \tau(\theta)\sin(\theta)\cos(\theta)d\theta. \quad (6)$$

On the other hand, frequency-dependent $\Lambda_{\mathrm{bulk}}$ was calculated from first-principles-based anharmonic lattice dynamics [28-30]. Details of RTMC and anharmonic lattice dynamics calculations are given elsewehere [24,29,30]. Here, we should note that the RTMC simulations is also capable of directly evaluating $\Lambda_{\mathrm{eff}}$ without resorting to Matthiessen's rule, which may be somewhat more accurate. As for the validity of the Matthiessen's rule, Hori, *et al.* have shown excellent agreement between results with and without Matthiessen's rule for polycrystalline silicon with random grain boundaries and lead telluride with rectangular nanopores [24,31]. Although this should certainly have limitation, particularly when directional scattering occurs at multiple interfaces with short distance between, in the current work, we used the Matthiessen's rule as it is much less computationally intensive and beneficial for handling complex systems such as the nano-porous structures.

## III. Results and Discussions

Figure 2 shows the volume-fraction dependence of thermal conductivity reduction for

randomly-placed spherical pores with different diameters. The effective thermal conductivity decreases with increasing volume fraction $\varphi$ and the reduction in thermal conductivity is enhanced by decrease in diameter. For a constant $\varphi$, as diameter decreases, scattering cross-section of a single spherical pore quadratically decreases, but the number of pores cubically increases. This gives rise to monotonous reduction of thermal conductivity as diameter decreases. As for the volume-fraction dependence, thermal conductivity rapidly decreases with increasing volume fraction from zero, and gradually saturates as volume fraction becomes larger. Therefore, an efficient strategy to reduce thermal conductivity would be to decrease the pore diameter while keeping their volume fraction low. This may be beneficial particularly in case of thermoelectric materials if electrons are transported diffusively and its reduction is dominantly determined by the volume fraction of pores. Here it is noted that the dependence of thermal conductivity on pore diameter is determined by the thermal conductivity spectrum of the material. The accumulation function of thermal conductivity of single crystal Si at 300 K obtained from first principles [29] (see Fig. A1 in the Appendix) shows that phonons with MFPs longer than 40 nm contribute to almost 90% of overall thermal conductivity. Thus, the thermal conductivity is largely reduced when the diameter of spherical pore is comparable to the onset MFP (~ 40 nm).

Figure 2 also compares the RTMC results with the theoretical models. As for macroscopic models such as Eucken model [11] and Bruggeman model [12,13], it is natural that these models do not reproduce RTMC results and underestimate the reduction of thermal conductivity since these do not account for the geometry of spherical pore and thus phonon ballisticity. Now we compare simulation results with the scattering model [19]. In Eq. (3), the scattering cross-sections at the limits of short-wavelength $\sigma_s$ is set to be $2\pi R^2$, where $R$ is the radius of spherical pore. The

long-wavelength scattering cross-sections, which corresponds to phonon-wave scattering, was ignored since a phonon is treated as particle in the RTMC simulation. Note that this is a reasonable assumption in reality for pores larger than several nanometers at room temperature because the nominal phonon wavelength is a few nanometers. Specifically, in this work, the minimum pore size was set to 10 nm, and the size is larger than wavelength of phonon contributing to heat conduction ranging from 0.03 to 6 nm. Meanwhile, averaged distance between two pores surfaces was 3.8 nm when the pore size was set to 10nm. Here, when considering phonon coherent length is comparable to wavelength of thermal excited phonons, nominal phonon coherent length in bulk silicon at room temperature is approximately 1 nm [32]. Therefore, other wave effects such as slit diffraction and localization, which could be an issue when the distance between surfaces of two pores becomes small at high volume fraction, are also ignored. In fact, Oyake *et al.*, showed that the phonon gas kinetic model can describe thermal conductivity of silicon nanocrystal with a diameter of 3 nm [33]. These simplifications reduce the scattering model to a general scattering model incorporating only the geometry, and thus we here address the model as the *geometrical scattering model* (GS model). Comparing RTMC results with the GS model, both are in good agreement in entire ranges of volume fractions and pore diameters. Furthermore, as seen from the comparison to the experiment [2], RTMC and GS model reasonably reproduce experimental results, which suggests the GS model is effective for explaining thermal conductivity reduction in nanoporous materials.

We next consider the diameter distribution of spherical pores. We defined the diameter distribution of spherical pore by a Gaussian function and evaluated how its standard deviation $\sigma$ affects the reduction of overall thermal conductivity. In the calculation, we fixed the mean

diameter as 100 nm and took the full diameter distribution into account for estimating porosity. Besides, random configuration of pore was considered. The result in Fig. 3 shows that the change in thermal conductivity with increase of $\sigma$ is small, and even with the distribution as wide as $\sigma$=0.75, variation from $\sigma$=0 is only a few percent. Such insensitivity of thermal conductivity to the diameter distribution has been already reported for grain size distribution in polynanocrystals [24] using the same RTMC simulations. As for the impact of pore alignment of spherical pores on heat conduction, as shown in Fig. 4, we confirmed that the pore alignment does not noticeably affect the thermal conductivity reduction either. Similar results have been obtained by previous Monte Carlo simulations for PbTe with nanopores [34]. These results show that effects of size distribution and alignment of spherical pore are small on thermal conductivity reduction.

Now an important question is whether the thermal conductivity would remain insensitive even with more complicated distributions. For this, we considered a system with bimodal distribution with two peaks at pore diameters that differ by an order of magnitude. In terms of thermal conductivity spectrum, a presence of bimodal diameter distribution can potentially affect phonons with specific and different ranges of MFPs. For instance, hierarchical nanostructuring, a combination of nanocrystalline structures and nanoparticle precipitation, has been experimentally demonstrated to noticeably reduce overall thermal conductivity [35]. Figure 5 shows volume ratio dependence of the thermal conductivity reduction for three different volume fractions. In these calculations, the two diameters were set to 20 nm and 200 nm. Note that although each peak has no distribution i.e. grain-size distribution is composed of two delta functions at 20 nm and 200 nm, this is equivalent to two peaks with significant width because thermal conductivity is insensitive to the peak width as discussed above. Thermal conductivity with bimodal pore

distribution monotonically decreases with the volume ratio of the smaller diameter pores to the larger ones since the number of spherical pores with smaller diameter increases. We further compare the RTMC results and GS model, where the scattering rates for two different diameters are summed as,

$$\Lambda_{\text{pore}}^{-1} = n_1\sigma_{s1}(d) + n_2\sigma_{s2}(D), n_1 = \frac{6\varphi\gamma}{\pi d^3}, n_2 = \frac{6\varphi(1-\gamma)}{\pi D^3}, \quad (7)$$

where $\gamma$ denotes the volume ratio of larger-diameter spherical pore. As seen in Fig. 5, the superposition of individual phonon-pore scattering reasonably explains the overall trend of RTMC results indicating. This result shows that the thermal conductivity reduction by bimodal pore distribution can be described by the GS model with average diameter of each mode. Namely, the single phonon-pore scattering is dominant in individual pore, and the effect of multiple phonon-pore scattering is not large. The above should be extendable to more number of peaks in the distribution and thus multi-modal systems in general.

We have so far considered spherical pores. Now we discuss the shape dependence by taking the case of randomly-placed rectangular pore as illustrated at Fig. 1(b). In the RTMC simulation, the rectangular pores were aligned along the cross-plane, i.e. normal to the heat flux. Figure 6 shows thermal conductivity reduction of nanoporous Si versus side length of rectangular pore ($a$). Monotonic reduction of thermal conductivity by both increase of volume fraction and decrease of side length can be explained in terms of total scattering cross-section increased by the number of pores, similar with the case of spherical pores. Unlike the spherical pore, scattering directivity or backward scattering is strong in the rectangular case, thus the GS model cannot be simply applied to the rectangular pores. Nevertheless, when regarding the rectangular pore as assembly

of cubic pores with effective scattering cross-section defined as $\sigma_s = \sqrt{2}a^2$, where $a$ denotes side length of the small cubic, thermal conductivity reduction can be described by the GS model, depending on porosity and side length.

We further calculated the spatial configuration dependence and influence of anisotropy of rectangular pores on thermal conductivity reduction, which are shown in Figs. 7 and 8, respectively. These results show that effect of pore alignment on thermal conductivity reduction is not negligible in contrast with the results of spherical pore, and the cubic alignment results in lower thermal conductivity than the hexagonal alignment. The difference should come from the difference in scattering directivity. On a rectangular pore, phonons are more frequently backscattered as illustrated in Fig. 6(c), whereas, on a spherical pore, phonons are more likely to be forwardscattered (Fig. 6(b)). Therefore, influence of spatial configuration in rectangular-pore systems on thermal conductivity reduction is larger than spherical pore systems. The results are consistent with the previous report [33]. Furthermore, the difference is enhanced by increasing porosity and side length of pore. As shown in Figs. 7 and 8, for high porosity and large side length, thermal conductivity reductions are less than the values calculated by the GS model. The cause of a discrepancy between RTMC and GS model can be due to the influence of multiple scattering. At high porosity and large side length limit where the distance between two interfaces become small, a phonon experiences multiple-scattering, and thus, each phonon-pore scattering can no longer be regarded as independent event and the GS model is no longer applicable. Even though the applicability of the GS model strongly depends on geometrical shape of pore, the GS model is useful for low porosity. In addition to size and alignment of rectangular pores, we investigate the effect of non-straight shape of rectangular pores on thermal conductivity reduction. As shown

in Fig. 9, tortuosity of rectangular pore weakens thermal conductivity reduction because the increase in total scattering cross-section projected to phonon propagation direction decreases; The total scattering cross-section is increased by tortuous in the vertical direction to heat flux, and, tortuous in parallel direction of heat flux does not change total scattering cross-section. In this case, although the GS model overestimates thermal conductivity reduction, it can be corrected by appropriately scaling the cross-section with the projected one as shown in Fig. 9.

## IV. Conclusion

In summary, we have evaluated impacts of pore geometry and distribution on thermal conductivity reduction by performing the RTMC simulations for nanoporous Si. As a result, we found that thermal conductivity of Si with spherical nanopores is mostly determined by total scattering cross-section that increases with decreasing size and increasing volume fraction. Presence of size distribution, even with multi-modal distribution, does not influence the reduction, which suggests that detailed structural manipulation in experiments would not lead to further thermal conductivity reduction. Considering other pore shapes namely rectangular pores with stronger directionality of surface phonon scattering, influence of spatial configuration on the thermal conductivity reduction is no longer negligible. On the technical side, RTMC results can be well reproduced by the GS model considering only geometrical scattering cross-section unless directional multiple phonon-pore scattering becomes important at high porosity. These findings provide practical means to understand and design thermal conductivity of nonporous materials not only for thermoelectrics but for heat transfer materials in general.

## Acknowledgements

This study is partially supported by Thermal Management Materials and Technology Research Association (TherMAT), TEPCO Memorial Foundation, JSPS KAKENHI (Grant No. JP16H04274), and JST CREST "Scientific Innovation for Energy Harvesting Technology" (Grant No. JPMJCR16Q5).

## Appendix

Figure A1 shows the accumulation function of thermal conductivity of bulk Si as a function of MFP calculated from first-principles-based anharmonic lattice dynamics[28-30].

## References


[1] H. J. Goldsmid, *Introduction to Thermoelectricity* (Springer, 2009).

[2] Z. Wang, J. E. Alaniz, W. Jang, J. E. Garay, and C. Dames, Thermal Conductivity of Nanocrystalline Silicon: Importance of Grain Size and Frequency-Dependent Mean Free Paths, Nano Letters **11**, 2206 (2011).

[3] M. Kashiwagi, S. Hirata, K. Harada, Y. Zheng, K. Miyazaki, M. Yahiro, and C. Adachi, Enhanced figure of merit of a porous thin film of bismuth antimony telluride, Applied Physics Letters **98**, 23114 (2011).

[4] D. W. Song, W. N. Shen, B. Dunn, C. D. Moore, M. S. Goorsky, T. Radetic, R. Gronsky, and G. Chen, Thermal conductivity of nanoporous bismuth thin films, Applied Physics Letters **84**, 1883 (2004).

[5] C. S. Sanmathi, Y. Takahashi, D. Sawaki, Y. Klein, R. Retoux, I. Terasaki, and J. G. Noudem, Microstructure control on thermoelectric properties of $Ca_{0.96}Sm_{0.04}MnO_3$ synthesised by co-precipitation technique, Materials Research Bulletin **45**, 558 (2010).

[6] P. K. Schelling, S. R. Phillpot, and P. Keblinski, Kapitza conductance and phonon scattering at grain boundaries by simulation, Journal of Applied Physics **95**, 6082 (2004).

[7] J. de Boor, D. S. Kim, X. Ao, M. Becker, N. F. Hinsche, I. Mertig, P. Zahn, and V. Schmidt, Thermoelectric properties of porous silicon, Applied Physics A **107**, 789 (2012).

[8] S. Tanaka, M. Takashiri, K. Miyazaki, and H. Tsukamoto, Thermoelectric Properties of Nano-Structured Bismuth Telluride Thin Films, in *2nd International Forum on Heat Transfer* (2008).

[9] M. Takashiri, S. Tanaka, H. Hagino, and K. Miyazaki, Combined effect of nanoscale grain size and porosity on lattice thermal conductivity of bismuth-telluride-based bulk alloys, Journal of Applied Physics **112**, 84315 (2012).

[10] J. Tang, H. T. Wang, D. H. Lee, M. Fardy, Z. Huo, T. P. Russell, and P. Yang, Holey silicon as an efficient thermoelectric material, Nano Letters **10**, 4279 (2010).

[11] Z. Hashin and S. Shtrikman, A Variational Approach to the Theory of the Effective Magnetic Permeability of Multiphase Materials, Journal of Applied Physics **33**, 3125 (1962).

[12] R. Landauer, The electrical resistance of binary metallic mixtures, Journal of Applied Physics **23**, 779 (1952).

[13] S. Kirkpatrick, Percolation and Conduction, Reviews of Modern Physics **45**, 574 (1973).

[14] J. K. Carson, S. J. Lovatt, D. J. Tanner, and A. C. Cleland, Thermal conductivity bounds for isotropic , porous materials, International Journal of Heat and Mass Transfer **48**, 2150 (2005).

[15] W. Kim and A. Majumdar, Phonon scattering cross section of polydispersed spherical nanoparticles, Journal of Applied Physics **99**, 084306 (2006).

[16] N. A. Katcho, N. Mingo, and D. A. Broido, Lattice thermal conductivity of $(Bi_{1-x}Sb_x)_2Te_3$ alloys with embedded nanoparticles, Physical Review B **85**, 115208 (2012).

[17] H. Zhang and A. J. Minnich, The best nanoparticle size distribution for minimum thermal conductivity, Scientific reports **5**, 8995 (2015).

[18] P. Chen, N. A. Katcho, J. P. Feser, W. Li, M. Glaser, O. G. Schmidt, D. G. Cahill, N. Mingo, and A. Rastelli, Role of surface-segregation-driven intermixing on the thermal transport through planar Si/Ge superlattices, Physical Review Letters **111**, 115901 (2013).

[19] A. Kundu, N. Mingo, D. A. Broido, and D. A. Stewart, Role of light and heavy embedded nanoparticles on the thermal conductivity of SiGe alloys, Physical Review B **84**, 125426 (2011).

[20] V. Jean, S. Fumeron, K. Termentzidis, S. Tutashkonko, and D. Lacroix, Monte Carlo simulations of phonon transport in nanoporous silicon and germanium, Journal of Applied Physics **115**, 24304 (2014).

[21] R. Dettori, C. Melis, X. Cartoixà, R. Rurali, and L. Colombo, Model for thermal conductivity in nanoporous silicon from atomistic simulations, Physical Review B **91**, 54305 (2015).

[22] M. F. Modest, *Radiative Heat Transfer, 2nd edtion* (Academic Press, Amsterdam; Boston, 2003).

[23] G. Chen, Phonon Wave Heat Conduction in Thin Films and Superlattices, Journal of Heat Transfer **121**, 945 (1999).

[24] T. Hori, J. Shiomi, and C. Dames, Effective phonon mean free path in polycrystalline nanostructures, Applied Physics Letters **106**, 171901 (2015).

[25] G. P. Srivastava, *The Physics of Phonons* (Taylor & Francis, 1990).

[26] J. M. Ziman, *Electrons and Phonons: The Theory of Transport Phenomena in Solids* (Oxford University Press, Oxford, New York, 2001).

[27] G. Chen, *Nanoscale Energy Transport and Conversion : A Parallel Treatment of Electrons, Molecules, Phonons, and Photons: A Parallel Treatment of Electrons, Molecules, Phonons, and Photons* (Oxford University Press, USA, 2005).

[28] D. A. Broido, M. Malorny, G. Birner, N. Mingo, and D. A. Stewart, Intrinsic lattice thermal conductivity of semiconductors from first principles, Applied Physics Letters **91**, 231922 (2007).

[29] K. Esfarjani, G. Chen, and H. T. Stokes, Heat transport in silicon from first-principles calculations, Physical Review B **84**, 085204 (2011).

[30] T. Tadano, Y. Gohda, and S. Tsuneyuki, Anharmonic force constants extracted from first-principles molecular dynamics: applications to heat transfer simulations, Journal of Physics: Condensed Matter **26**, 225402 (2014).

[31] T. Hori, Ph.D Thesis, The University of Tokyo, 2015.

[32] R. Prasher, Ultralow thermal conductivity of a packed bed of crystalline nanoparticles: A theoretical study, Physical Review B **74**, 165413 (2006).

[33] T. Oyake, L. Feng, T. Shiga, M. Isogawa, Y. Nakamura, and J. Shiomi, Ultimate Confinement of Phonon Propagation in Silicon Nanocrystalline Structure, Physical Review Letters **120**, 45901 (2018).

[34] T. Hori, G. Chen, and J. Shiomi, Thermal conductivity of bulk nanostructured lead telluride, Applied Physics Letters **104**, 21915 (2014).

[35] K. Biswas, J. He, I. D. Blum, C.-I. Wu, T. P. Hogan, D. N. Seidman, V. P. Dravid, and M. G. Kanatzidis, High-performance bulk thermoelectrics with all-scale hierarchical architectures, Nature **489**, 414 (2012).

**Figures**

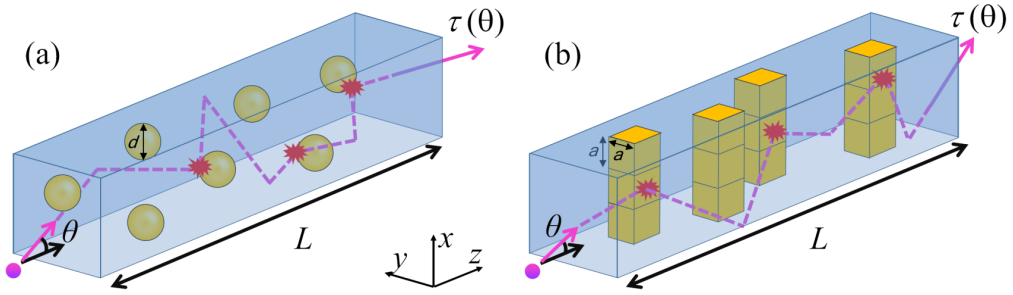


**Fig. 1** A schematic of phonon transport in nanoporous Si with different type of pores (a) spherical pore and (b) rectangular pore, respectively. Phonon transmittance calculation by Ray-tracing Monte Carlo (RTMC) simulation is illustrated in (a). Phonon is incident on *x*-*y* plane at $z$=0 with azimuthal angle $\varphi$ and polar angle $\theta$. Transmittance $\tau$ is calculated by counting the number of phonons reaching on *x*-*y* plane at $z$=$L$. Phonon-pore scattering is treated as diffusive, and perfect specular boundary condition is applied along *x*- and *y*-directions. $d$ and $a$ denote a diameter of spherical pore and side length of rectangular pore, respectively.

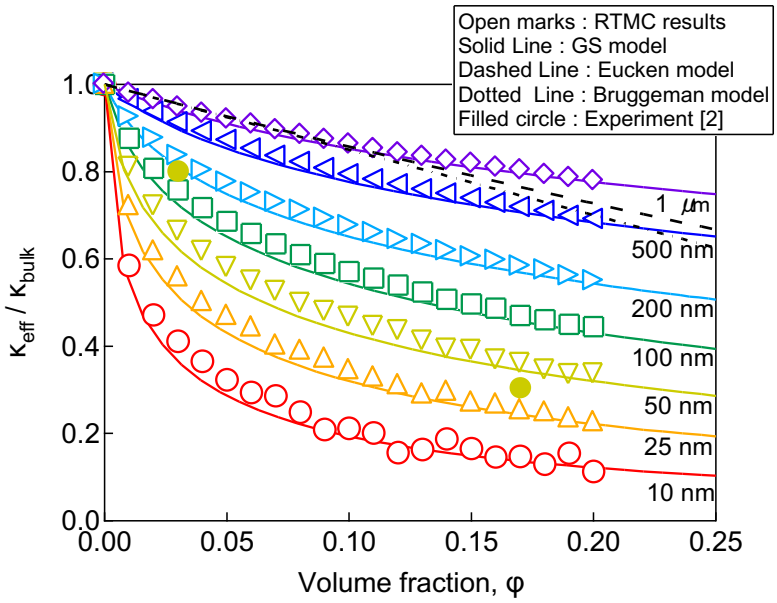


**Fig. 2** Volume fraction dependence of effective lattice thermal conductivity ($\kappa_{eff}$) of nanoporous Si at 300 K for spherical pores with different diameters. $\kappa_{bulk}$ denotes the thermal conductivity of bulk Si. Dashed and dotted lines are results of Eucken model [11] and Bruggeman model [12,13]. Solid lines denote geometrical scattering (GS) model [Eq. (3)] [16,19]. Filled circles are experimental results previously reported [2].

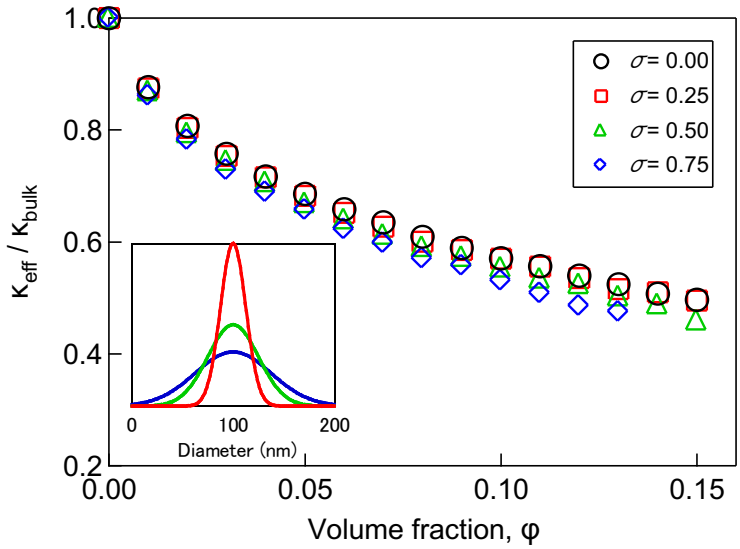


**Fig. 3** Impact of diameter distribution of randomly located spherical pores on thermal conductivity reduction of nanoporous Si at 300 K. The standard deviation $\sigma$ of Gaussian for diameter distribution is varied as 0 (black open circle), 0.25 (red open square) 0.5 (green open triangle), and 0.75 (blue open diamond). Mean diameter is set to 100 nm.

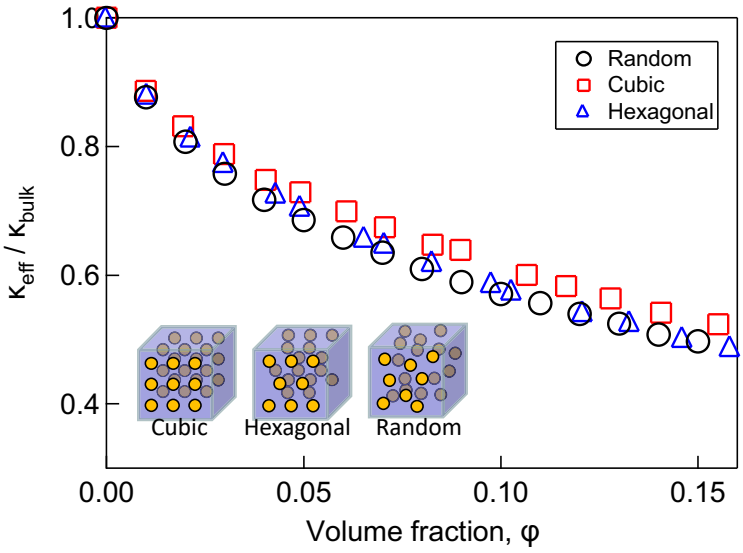


**Fig. 4** Impact of alignment of spherical pores on thermal conductivity reduction of nanoporous Si at 300 K. Three different configurations (random, cubic, and hexagonal) considered in this calculation are illustrated in the inset figure. In this calculation, the diameter of spherical void is fixed to 100 nm.

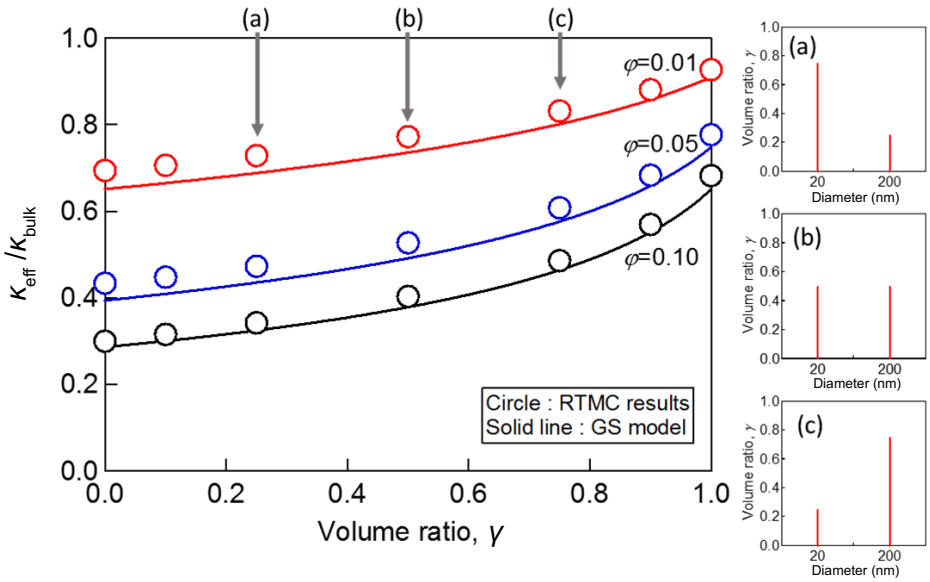


**Fig. 5** Influence of the bimodal distribution on thermal conductivity of nanoporous Si at 300 K for different volume fractions. The open circles and solid lines are results from RTMC and GS model calculations, respectively.

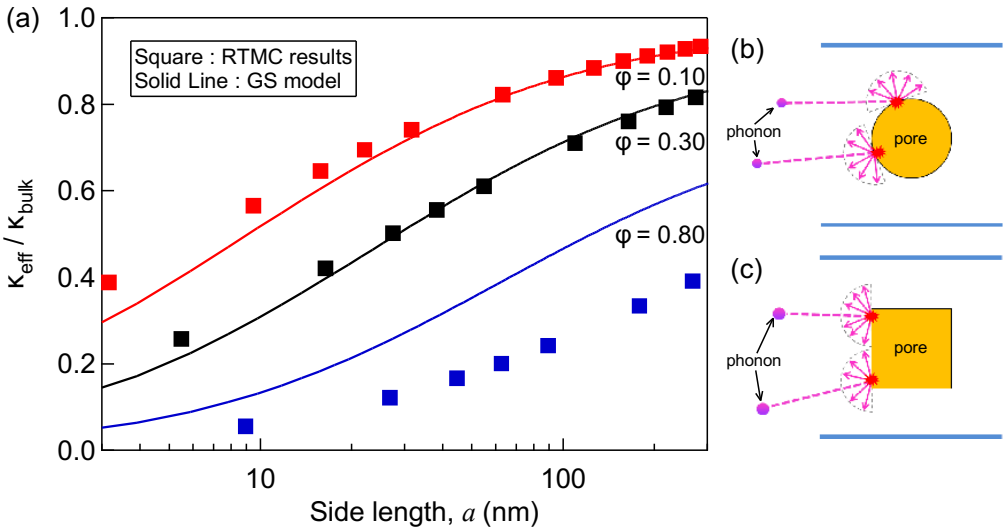


**Fig. 6** (a) Side-length dependent $\kappa_{eff}$ of nanoporous Si at 300 K for randomly-placed rectangular pores with different volume fraction (red: 10%, black: 30%). Squares and solid lines are results of RTMC simulation and GS model, respectively. (b) A schematic of phonon-pore scattering with spherical void, (c) A schematic of phonon-pore scattering with rectangular void.

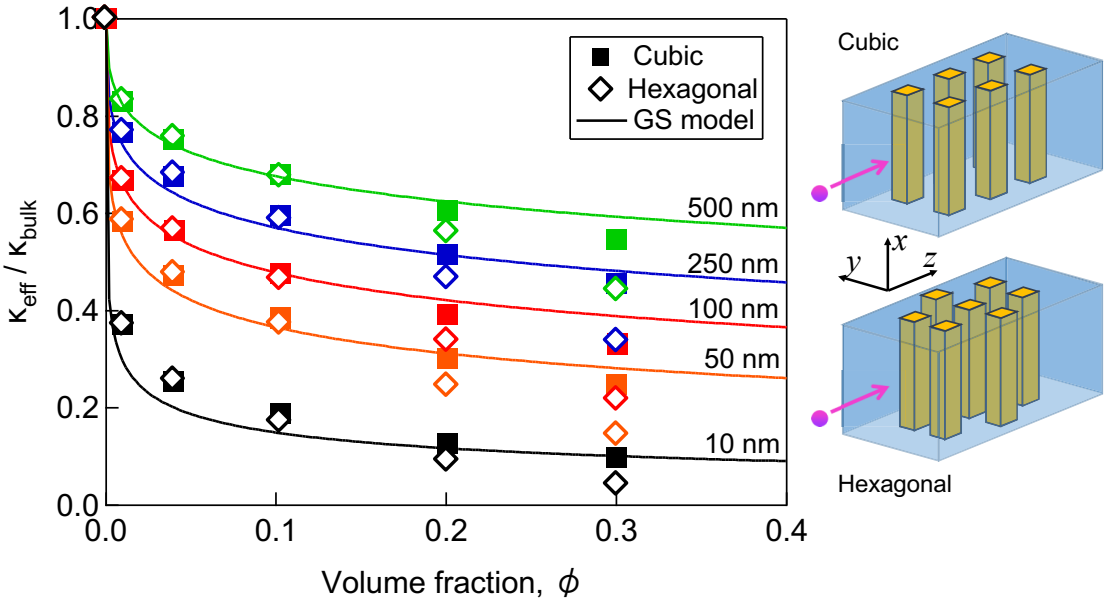


**Fig. 7** Impact of alignment of rectangular pore on thermal conductivity reduction calculated by RTMC simulation. Squares and diamonds are results of RTMC simulation with cubic alignment and hexagonal alignment, respectively. Solid lines are results of RTMC simulation and GS model, respectively.

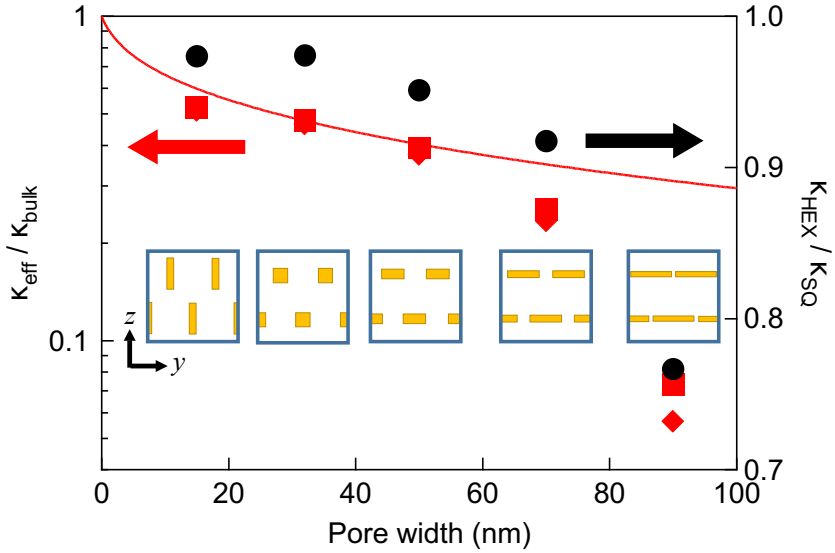


**Fig. 8** Impact of pore width of rectangular pore on thermal conductivity reduction calculated by RTMC simulation. Squares and diamonds are results of RTMC simulation with cubic alignment and hexagonal alignment, respectively. Solid lines are results of RTMC simulation and GS model, respectively. Circles are a ratio of calculated thermal conductivity of hexagonal and cubic alignment.

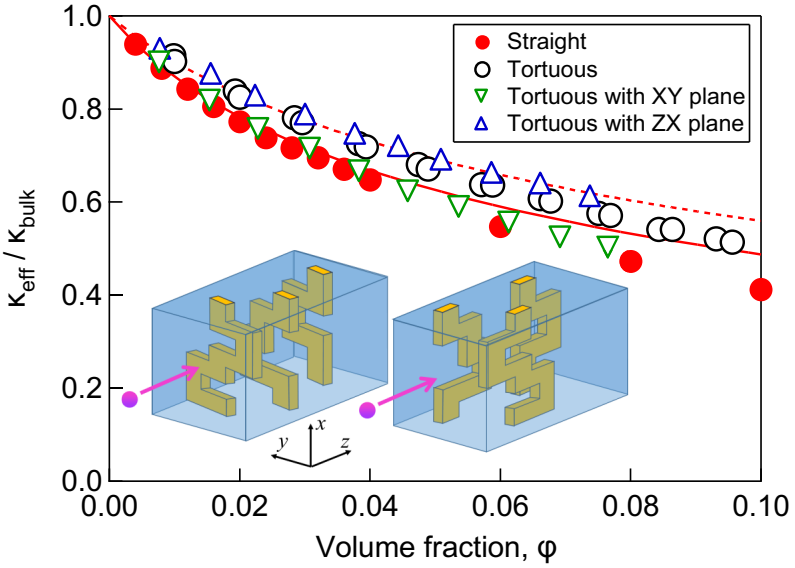


**Fig. 9** Impact of tortuous on thermal conductivity reduction calculated by RTMC simulation. Four different configurations are considered (straight, random tortuous, tortuous with *x*-*y* plane, and tortuous with *z*-*x* plane) as illustrated in the inset. Solid line and dashed line are

results of GS model and modified GS model in consideration of actual scattering cross-section on tortuous structure, respectively. In this calculation, the side length of rectangular void is fixed to 100 nm.

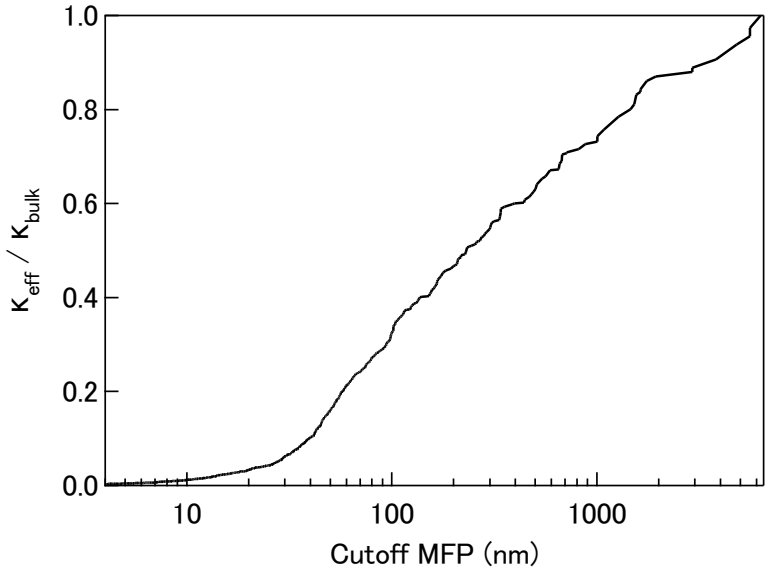


**Fig. A1** Normalized cumulative thermal conductivity of bulk Si at 300 K calculated from first-principles-based anharmonic lattice dynamics [29].